Analytica Chimica Acta 1374 (2025) 344519

Contents lists available at ScienceDirect

Analytica Chimica Acta

journal homepage: www.elsevier.com/locate/aca

Disposable electrochemical aptasensor for rapid and selective vancomycin detection in clinical samples: Bridging affinity selection, computational modeling and clinical validation

Magdolna Casian [a,b,c], Oana Hosu-Stancioiu [a], Ioana Manea [a], Dimas Suárez [b], Natalia Díaz [b], María Jesús Lobo Castañón [b,c], Noemí de-los-Santos-Álvarez [b,c,*], Cecilia Cristea [a,**]

[a] Department of Analytical Chemistry, Faculty of Pharmacy, Iuliu Haţieganu University of Medicine and Pharmacy, 4 Pasteur Street, 400349, Cluj-Napoca, Romania
[b] Departamento de Química Física y Analítica, Universidad de Oviedo, Av. Julián Clavería 8, 33006, Oviedo, Spain
[c] Instituto de Investigación Sanitaria del Principado de Asturias, Av. de Roma s/n, 33011, Oviedo, Spain

HIGHLIGHTS

- MB-SELEX enriches aptamers faster than capture SELEX and with similar affinity.
- The 45 nt aptamers were characterized by surface plasmon resonance.
- The 3D structure of aptamer and vancomycin complex was computationally predicted.
- The electrochemical aptasensor allows vancomycin detection in clinical samples.
- The aptasensor performance is comparable to that of the standard immunoassay.

GRAPHICAL ABSTRACT

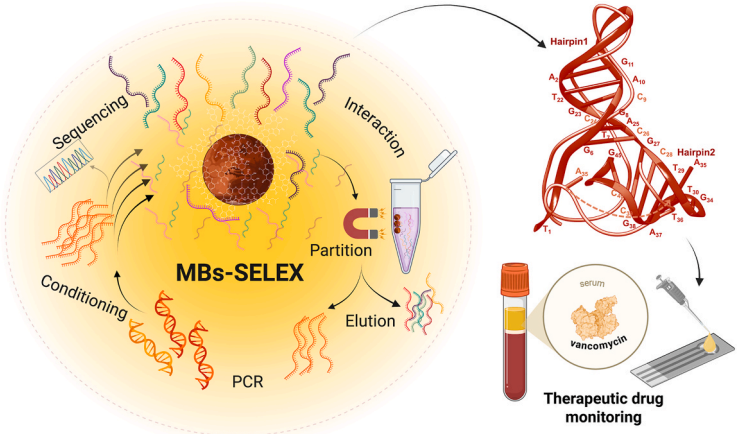

ARTICLE INFO

Handling Editor: Prof Nicola Cioffi

Keywords:
Aptamer
Magnetic bead SELEX

ABSTRACT

Antibiotic resistance is a growing global threat, with glycopeptides like vancomycin remaining critical for treating resistant infections. However, its narrow therapeutic index necessitates therapeutic drug monitoring (TDM). In this study, we present a disposable electrochemical aptasensor for cost-effective and rapid vancomycin monitoring. Novel high-affinity aptamers were identified via magnetic bead-based SELEX, with their binding

* Corresponding author. Departamento de Química Física y Analítica, Universidad de Oviedo, Av. Julián Clavería 8, 33006, Oviedo, Spain.
** Corresponding author.
E-mail addresses: magdolna.casian@elearn.umfcluj.ro (M. Casian), hosu.oana@umfcluj.ro (O. Hosu-Stancioiu), ioana.manea@elearn.umfcluj.ro (I. Manea), dimas@uniovi.es (D. Suárez), diazfnatalia@uniovi.es (N. Díaz), mjlc@uniovi.es (M.J. Lobo Castañón), santosnoemi@uniovi.es (N. de-los-Santos-Álvarez), ccristea@umfcluj.ro (C. Cristea).

https://doi.org/10.1016/j.aca.2025.344519
Received 10 April 2025; Received in revised form 30 July 2025; Accepted 6 August 2025
Available online 6 August 2025

Vancomycin
APTAMD software
Molecular docking
Electrochemical aptasensor
Clinical serum monitoring

confirmed by surface plasmon resonance and computational modeling. The aptasensor, developed on screen-printed gold electrodes using a multipulse-assisted immobilization method, demonstrated a linear response from 2.5 to 50 μM and a detection limit of 1.5 μM. This range encompasses clinically relevant trough (10–13.5 μM) concentrations. Validated in undiluted clinical samples, it showed performance comparable to gold-standard immunoassays, offering a promising tool for vancomycin TDM.

1. Introduction

The global threat of antibiotic resistance is a major public health concern resulting from antibiotic misuse and unsuccessful development of novel and effective antimicrobial agents [1,2]. The increasing prevalence of antibiotic-resistant Gram-positive and Gram-negative bacteria and antibiotic-resistance genes in the microbiome has necessitated the effective management of antimicrobial therapies [3].

Therapeutic drug monitoring (TDM) is a critical tool in the management and individualization of antibiotic therapy that relies on real-time dose adjustment by measuring the drug concentration in biological fluids to enhance the safety and effectiveness of treatment [4].

First discovered in the 1950s, glycopeptide antibiotics, such as vancomycin (Van), remained the key drugs for the treatment of severe infections caused by Gram-positive pathogens, such as methicillin-resistant *Staphylococcus aureus* and *Clostridium difficile* [5]. Having a narrow therapeutic index, one of the major concerns of exposure to Van is the occurrence of nephrotoxicity, ototoxicity and the most known "red man syndrome" [6]. Van has concentration and time–dependent antimicrobial activity, therefore understanding the pharmacokinetic (biodistribution after exposure) and pharmacodynamic (minimum drug concentration that inhibits bacterial growth; MIC) properties is crucial for the correct management of therapy [3]. In clinical laboratories, there are two main indicators of the outcomes of a positive treatment: i) the ratio of the area under the plasma concentration-time curve during a 24 h time period (AUC0-24) and the MIC (AUC0-24/MIC should be $\geq$ 400) and ii) the trough levels of Van in serum that should be between 15 and 20 mg/L, as concentrations under 10 mg/L promote the development of antibiotic resistance [7,8].

Routine Van assessment in clinical laboratories is based on commercially available assays, such as chemiluminescence immunoassay [9], fluorescence polarization immunoassay [10], kinetic interaction of microparticles in solution [11], enzyme-multiplied immunoassay [12], particle-enhanced turbidimetric inhibition immunoassay [13] or high-performance liquid chromatography coupled with mass spectrometry [14–16]. These techniques have certain limitations, including variability in accuracy across different methods, the need for sophisticated instruments, cross-reactivity, and prolonged analysis time ranging from hours to days [7].

Aptamers are short, single-stranded DNA or RNA sequences screened *in vitro* through a process called systematic evolution of ligands by exponential enrichment (SELEX). Since their discovery in the early 1990 [17,18], aptamers have come into the spotlight as an innovative and appealing alternative to antibodies as biorecognition elements in terms of stability, ease of synthesis and functionalization, structural consistency between batches and suitability for a wide variety of target molecules [19].

After more than three decades of research and innovation, various SELEX methods have been developed for the selection of high-affinity nucleic acid aptamers, like capillary electrophoresis-SELEX [20], cell-SELEX [21], microfluidic chip SELEX [22] and solid phase carrier-SELEX [23,24].

Magnetic beads-based SELEX (MBs-SELEX), a sub-type of solid phase carrier-SELEX has significantly enhanced the limitations of conventional selection technology, in terms of efficiency and rapidity. MBs are useful solid supports for the immobilization of targets during aptamer selection because they enable fast and efficient partitioning of small-volume samples [25].

The first Van-specific aptamer reported in the literature was selected by Capture SELEX using streptavidin-coated columns as the support for the DNA random library [26]. This SELEX procedure oriented to obtain strong conformational switching aptamers requires expensive, time-consuming post-SELEX truncation steps to destabilize the full-length aptamer to achieve a significant signal gain. The 3-base paired truncated version (K_D = 19.5 ± 1.6 μM) highlighted the necessity of including consideration of human matrix effects into future selection strategies [27]. To address this, our selection protocol was designed to integrate two key approaches: (1) enrichment of the selection buffer with bovine serum albumin (BSA) and transfer RNA (tRNA) to better mimic the complex serum matrix and enhance a more competitive selection, and (2) introduction of a counter-selection step using teicoplanin (Teico), a structural analog of Van. This approach is based on the premise that selecting an aptamer capable of discriminating between structural analogs will yield highly specific Van aptamers, thereby mitigating any concerns related to selectivity and potential multiple-target binding events.

The affinity of the selected aptamers was evaluated by surface plasmon resonance (SPR). For a more comprehensive understanding of aptamer-target binding, the structure of 8H aptamer and its complex with Van was computationally predicted using molecular dynamics and docking calculations. To further prove the binding of the selected aptamer, a disposable, label-free electrochemical sensor was also developed on screen-printed gold electrodes (AuSPE). The aptasensor was validated in serum samples collected from hospitalized patients undergoing Van treatment.

2. Experimental section

Reagents and instrumentation are detailed in Supplementary Information (SI).

2.1. SELEX protocol

The selection of Van-specific aptamers was carried out using a single-stranded DNA library of randomized sequences, a central region with 45 random nucleotides and two constant regions at the 5' (18 nt) and 3' (25 nt) ends that acted as a hybridization zone for the PCR primers. The sequences of the DNA library and the PCR primers are indicated in Table S1. Each round of selection included the following steps: i) interaction between 1 nmol of DNA library (first round) or 250 pmol in the following rounds with 100 μL ethanolamine-modified MBs (MBs-EtAm) (negative selection) and then the supernatant was incubated with MBs-Van (positive selection). From round 5 a counter selection step with MBs-Teico was introduced prior to positive selection; ii) magnetic separation of unbound sequences and elution from the complex at 95 °C in water; iii) PCR amplification and iv) strand separation using streptavidin-modified MBs under alkaline conditions. Stringency was increased according to Table S2. Detailed protocol on MBs preparation and SELEX protocol including cloning, sequencing and bioinformatic analysis are provided in SI.

2.2. Affinity evaluation of the unmodified aptamers

Initially, the bare gold-coated glass sensor was cleaned by immersion in piranha solution ($3H_2SO_4$ (95 %): $1H_2O_2$ (33 %)) for 3 min, thoroughly rinsed with water and ethanol, and dried with a stream of N_2.

The self-assembled thiol monolayer (SAM) was prepared by covering the Au disc with 200 μL of a mixture containing 0.25 mM 11-mercaptoundecanoic acid (MUA) and 0.75 mM 6-mercapto-1-hexanol (MCH) in ethanol and left overnight at 4 °C in ethanol-saturated atmosphere. The sensor with the carboxylic SAM was rinsed with ethanol and dried under a stream of N_2 and positioned onto a clean hemi-cylinder lens previously coated with a drop of immersion oil (Cargille Certified Refractive Index Liquid, refractive index 1.5142 ± 0.0010). Afterwards, both channels were washed three times with 70 μL of water, and the surface was equilibrated with modification buffer (10 mM sodium acetate pH 5.5) until a constant response was obtained.

The immobilization of Van onto the SAM on gold consisted in a three-step sequence: (1) Surface activation: three consecutive injections of a mixture of 0.2 M N-(3-dimethylaminopropyl)-N′-ethylcarbodiimide hydrochloride and 0.05 M N-hydroxysuccinimide in water for 10 min each one. (2) Binding step: three consecutive injections of 10 mM Van in 0.1 M N-(2-hydroxyethyl)piperazine-N′-(2-ethanesulfonic acid) buffer, pH 8.3 in the signaling channel and 1 M EtAm in phosphate buffer saline (PBS), pH 7.4 in the reference channel for 20 min each one. (3) Blocking step: one injection of 1 M EtAm prepared in PBS, pH 7.4 in both channels for 30 min. Brief washing with modification buffer was performed between steps. Finally, the modified surface was equilibrated with PBS, pH 7.4; (affinity solution, the buffer used in the selection) and used for the binding experiments.

The full experiment consisted of recording successive independent cycles of measurement: baseline provided the initial angle (m°i), injection of varying concentrations of aptamer prepared in affinity buffer (35 μL) in both channels, for 20 min (association phase) and after draining the cuvette, injection of 50 μL of affinity buffer to record the dissociation phase for 5 min (final angle, m°f). For each injected concentration, the difference in the angle change was calculated as $\Delta m^\circ = m^\circ f - m^\circ i$ at each channel. The net angle change was obtained by difference between the signaling and the reference channels.

2.3. Affinity evaluation of the immobilized aptamer

For the SPR setup, the bare Au chip was initially washed with ethanol, dried under a nitrogen stream, and hydrated with 300 μL PBS buffer for 1 h at RT. The Au chip was then covered with 300 μL of 1 μM 8H_1 solution prepared in the same buffer and left overnight at 4 °C in a water-saturated atmosphere. The surface was washed with 300 μL of PBS buffer and incubated with 300 μL of 100 μM MCH in PBS for 30 min, at RT. After washing the excess MCH with 300 μL PBS, the prepared chip was mounted on the SPR prism and used for the experiments, with PBS as the running buffer at a constant flow rate of 60 μL/min. Prior to analysis, the running buffer was filtered through a 0.2 μm pore diameter filter and degassed for 1 h under vacuum (25 inHg) at 25 °C using a Degassing Station (TA Instruments).

After obtaining a stable baseline, the PBS buffer was injected for blank correction, and then 300 μL of 1–25 μM Van concentrations prepared in PBS were injected for 300 s (association phase), followed by 300 s of running buffer through the system before a new injection (dissociation phase and new baseline stabilization). All kinetic analyses of aptamer binding were performed by fitting the data to the Langmuir equation ($R=R_{max} \times C/(K_D + C)$, where R and R_{max} are the angle shift and the maximum angle shift, respectively, K_D is the dissociation constant and C the Van concentration, assuming a 1:1 interaction.

2.4. Computational modelling and docking

The molecular dynamics (MD) model of the 8H sequence in explicit solvent was built using the APTAMD computational protocol [28]. We used first the mfold algorithm to predict the 8H secondary structure, and the resulting 2D model was transferred to the RNA-COMPOSER tool to generate an initial 3D RNA model, which was transformed into the equivalent DNA molecule, minimized, and solvated using the AMBER suite of programs [29]. Finally, the conformational space accessible to 8H was sampled by 2.5 μs of Gaussian-accelerated Molecular Dynamics (GaMD), followed by 10.0 μs of conventional Molecular Dynamics (cMD) to characterize the equilibrium properties of the aptamer. Further details about the protocol and the detailed settings can be found in the SI.

Docking calculations were conducted using Autodock 4.2 [30], following a semi-rigid docking protocol that allowed the internal rotation about twenty-three single bonds of Van. To introduce some degree of flexibility in the aptamer, a series of Autodock calculations were performed using the aptamer coordinates retrieved from the twelve most populated clusters provided by the cMD simulation. In this way, we obtained a total of 12 × 250 different poses for the 8H-Van complex, and the 300 most favorable ones were subjected to geometry relaxation to remove bad contacts and finally reranked in terms of the Autodock scoring function.

2.5. Detection of Van on aptamer-modified AuSPE

The detection of Van with the aptasensor involved three main steps following AuSPE conditioning: (1) aptamer immobilization via covalent Au-thiol bonding; (2) blocking of the remaining active Au surface sites with *p*-aminothiophenol (*p*-ATP); (3) incubation with the target in affinity buffer for 30 min; and (4) electrochemical detection by differential pulse voltammetry (DPV) in the presence of 5 mM $[Fe(CN)_6]^{3-/4-}$ solution in 0.1 M KCl. A detailed protocol is provided in SI.

The analytical signal was determined by measuring the decrease in the current intensity ($\Delta I/I_0$ (%)) after Van interaction, based on the anodic current intensity before (I_0) and after (I) incubation, using the following equation:

$$\frac{\Delta I}{I_0}\,(\%) = \frac{(I_0 - I) \times 100}{I_0} \quad (1)$$

2.6. Analysis in human serum

Recovery studies were performed with spiked commercial human serum, pre-filtered through 0.45 μm syringe filter. Van concentration in the spiked samples was determined in triplicate using the DPV calibration curve, and recovery rates were calculated.

Additionally, undiluted serum samples from ten patients undergoing Van treatment at Cluj-Napoca Municipal Clinical Hospital were analyzed with the aptasensor as indicated for the spiked samples and validated with a homogeneous particle-enhanced turbidimetric inhibition immunoassay (PETINIA) using Multigent Vancomycin assay kit. Further details are provided in SI.

3. Results and discussions

3.1. Screening of Van-binding aptamers

The amount of target used in SELEX is important though there is not rule of thumb to make the decision. In MBs-SELEX high loading can yield aptamers that bind simultaneously to two or more targets while low loading can yield to SELEX failure due to excessive stringency. As a compromise, we experimentally determined that a Van concentration of 20 mM yields approximately a monolayer of immobilized Van (Figures S1 and S2). The SELEX procedure on MBs-COOH involved the interaction with 1 nmol of ssDNA in the first round and 250 pmol in the following ones, maintaining a 10:1 ratio (DNA: target). The incubation time and number of washing steps were gradually varied throughout the rounds to increase the stringency of selection, as shown in Table S2. Negative steps were performed prior to each positive selection while counter selection steps with MBs-Teico were initiated in the fifth round. BSA and tRNA were added to the selection buffer to mimic the physiological conditions of human serum and enhance the selection stringency.

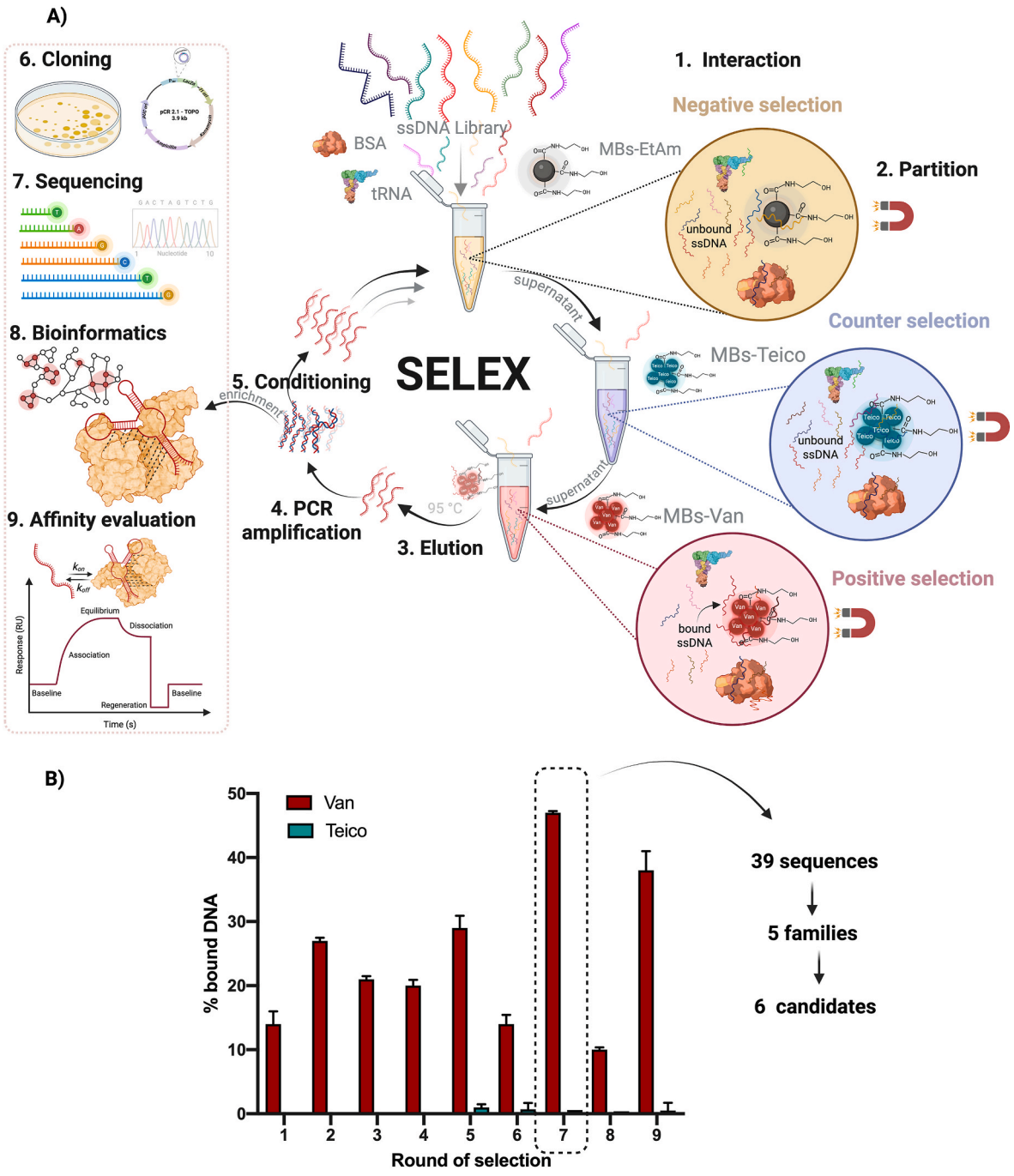

Fig. 1. A) Schematic representation of the SELEX process for Van aptamer selection and characterization, including all the key steps: (1) interaction of the ssDNA library with MBs-EtAm (negative selection), MBs-Teico (counter selection from round 5), and MBs-Van (positive selection); (2) partitioning; (3) elution; (4) PCR amplification; (5) conditioning; (6) cloning; (7) Sanger sequencing; (8) bioinformatic analysis and motif search; and (9) affinity evaluation. **B)** Enrichment analysis: bound percentages of ssDNA from each SELEX round towards Van and Teico, determined by UV-VIS spectroscopy at 260 nm. Created with Biorender.com.

Fig. 1A provides an overview of the main steps and conditions used in the nine rounds of selection.

The enrichment process and the effectiveness of the counter-selection step were monitored using UV-VIS spectroscopy at 260 nm, by calculating the percentage of DNA strands bound to MBs-Van and MBs-Teico, respectively. Fig. 1B illustrates a progressive enrichment of Van-binding sequences across the SELEX rounds, with the highest binding percentage observed in round 7. This round yielded a maximum binding of 47 % towards Van, indicating satisfactory sequence enrichment, while maintaining minimal binding to Teico (<1 %), thereby demonstrating high selectivity of the potential aptamer candidates. A decrease in Van-bound percentage was observed after increasing the washing steps to 5 × (round 6) and reducing the incubation time from 30 min to 15 min (round 8). Nevertheless, round 9 (conducted under the same conditions as round 8) showed a partial recovery of binding (38 %), although still lower than that observed in round 7. Consequently, round 7 was selected for cloning and sequencing, as it offered an optimal balance between high binding affinity and selectivity under practical assay conditions (30 min incubation), supporting the potential applicability of the selected aptamers.

Gel electrophoresis of individual clones showed the presence of two products (Figure S3). Sequencing demonstrated that the shorter

fragments were primer-dimers, while the longer fragments corresponded to the expected 88 bp PCR product. The long sequences were further analyzed with bioinformatic tools for homology and repetitive motifs. Prior to starting the *in silico* analysis, the primer regions were truncated. The phylogenetic tree obtained with the Galaxy online tool (Figure S4) allowed dividing the sequences into five distinct families (A – E). Using Meme Suite software, we found 11 recurrent motifs present in more than three sequences (Table S3). Figure S5 shows the multiple sequence alignment (Galaxy), the location of motifs in each sequence and the Gibbs free energy of the most stable structure as estimated with mfold web server [31]. Together this information allowed us to select six candidates (bold and underlined), whose structures are shown in Fig. 2A (Family A–7G, Family B–8H, Family D–9F and 11D, and Family E–6C and 3C).

3.2. Affinity evaluation of aptamers by SPR

The affinity of the six aptamers selected was interrogated by SPR. Initially, to maximize the SPR signal, the small molecule (Van) was immobilized onto a mixed SAM containing carboxylic groups (Fig. 3A). The nonspecific adsorption was evaluated in the reference channel where only EtAm was anchored and subtracted from the Van channel.

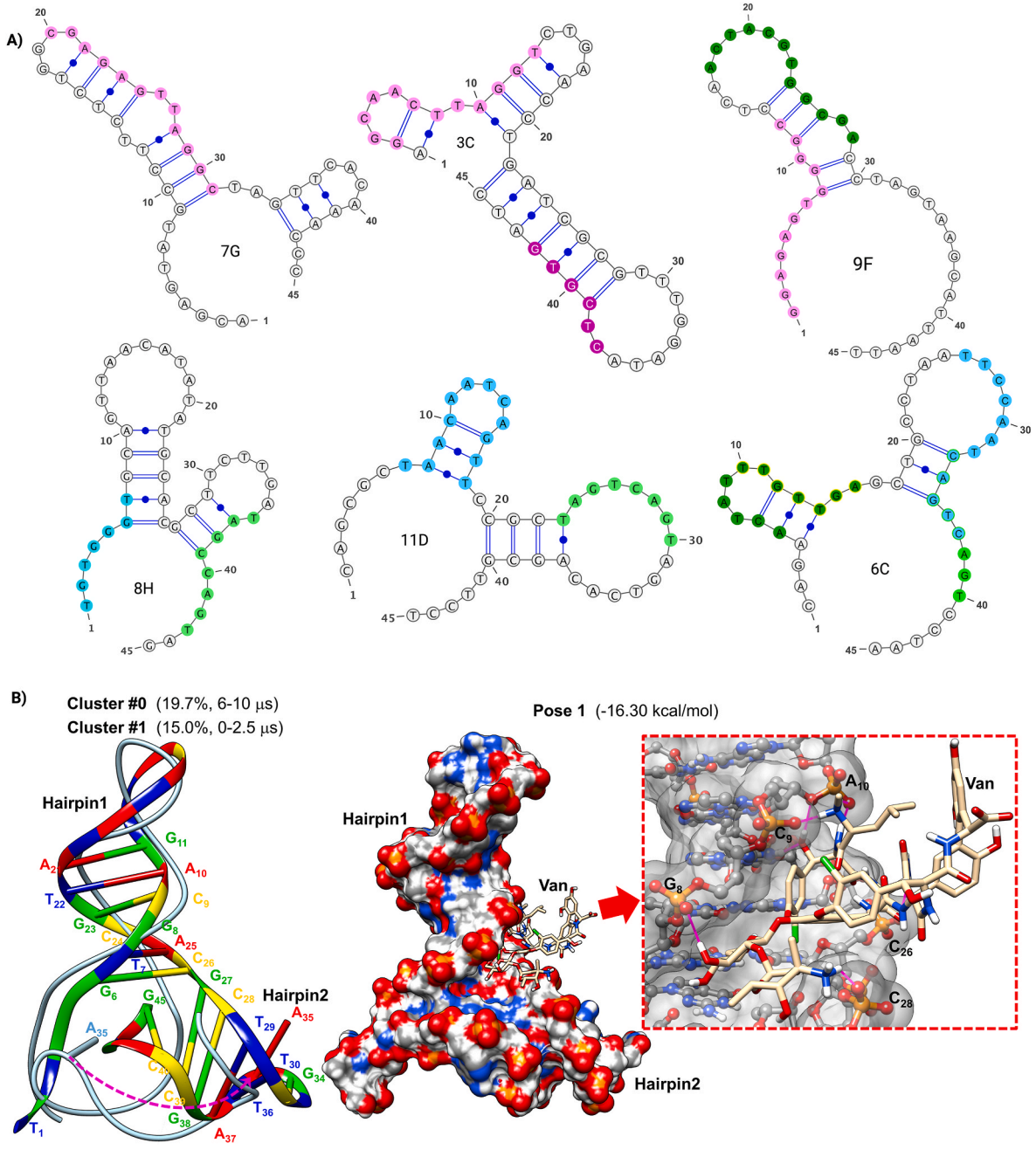

Fig. 2. A) *In silico* prediction of the most stable secondary structures for six candidate aptamers selected via bioinformatic screening, highlighting their most representative motifs. Structures were obtained with mfold [31] and displayed with Varna [32], under the following conditions: 25 °C, 0.150 M Na^+. **B)** Superposition of ribbon models for the 3D structure of 8H in the two most abundant clusters, with nucleobases involved in stable base pairs represented as sticks in cluster #0. The dashed magenta line and the stick corresponding to nucleobase A35 highlight the displacement of hairpin 2 during the simulation. Most favored pose obtained for the 8H-Van complex with the aptamer represented as a surface colored according to atom types and the ligand as sticks. Detailed view of some of the 8H●●●Van contacts (lines in magenta). Only polar H atoms are displayed.

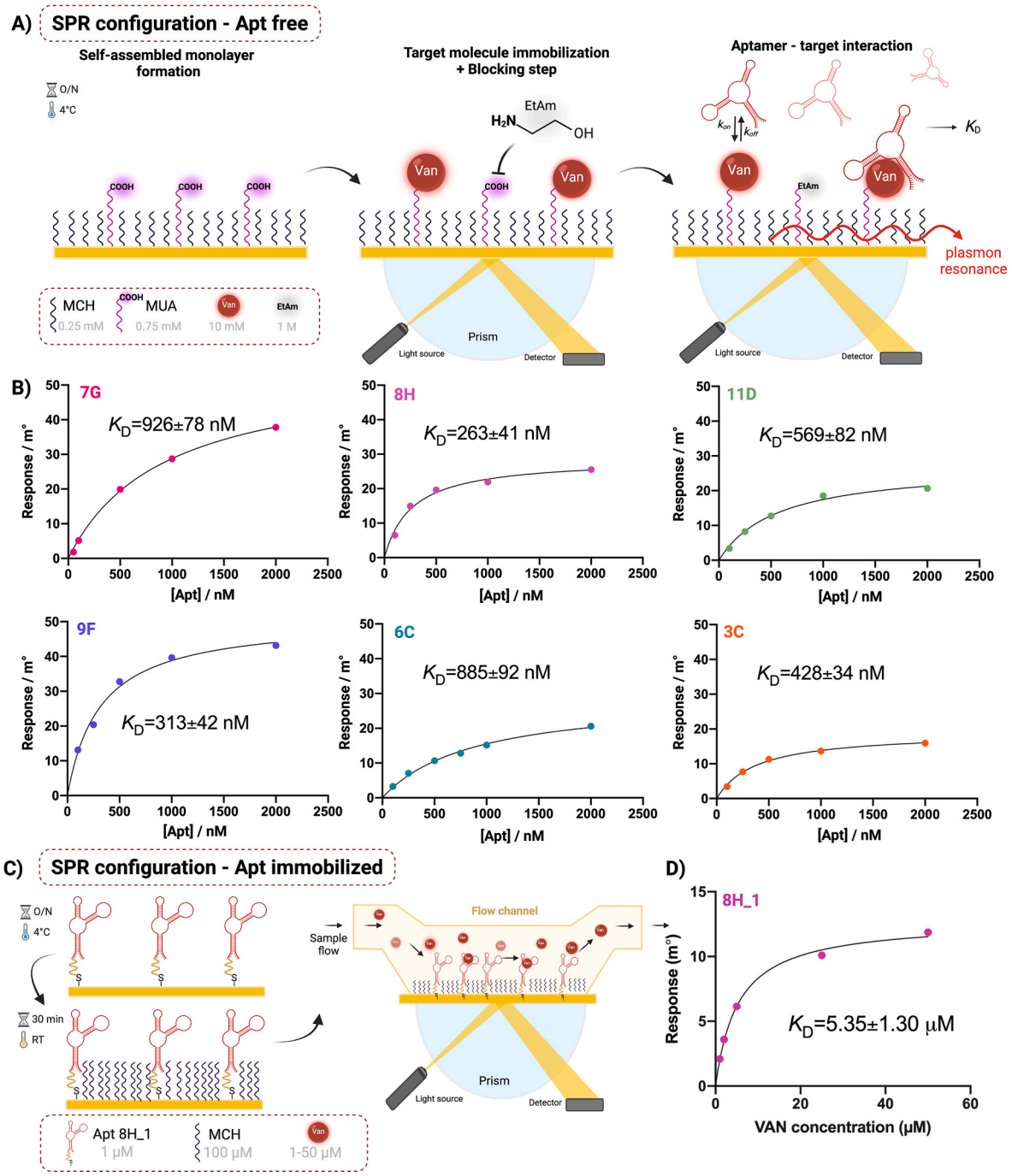

Fig. 3. Schematic representation of the SPR setup with the immobilization of **A)** Van and **C)** the aptamer on the sensor surface. Binding isotherms obtained using a **B)** Van-modified sensor after interaction with increasing concentrations of Apt (100–2000 nM) and **D)** Apt-modified sensor after interaction with increasing concentrations of Van (1, 2, 5, 25, and 50 µM).

After obtaining a stable baseline, increasing concentrations of each aptamer were injected (100–2000 nM) and a binding curve was plotted and fitted to the Langmuir model, assuming a one-to-one interaction (Table S4). The K_D of all six aptamers were then calculated (Fig. 3B).

All aptamers show subµM K_D values. Aptamers 8H and 9F showed the highest affinity, 263 ± 41 nM and 313 ± 43 nM, respectively. Considering the uncertainty, both aptamers exhibit equal affinity; however, aptamer 9F showed 1.75-fold higher maximum angle shifts, suggesting that the binding site of Van is more accessible than that of 8H in this surface architecture. Note that the Van surface coverage range obtained in these experiments does not correlate with the K_D values, ruling out overlap as a cause of fewer bound aptamers. It is also worth noting that the sequences with the strongest secondary structures (3C and 7G) were not the best binders. While some aptamers share several motifs, we did not find any preferable motif as we reported previously [33].

To assess the capture ability of the selected aptamer, a configuration using aptamer 8H_1 anchored through the Au–S chemistry in a binary SAM with MCH as antifouling agent was tested, although much smaller signals were expected due to the small size of the antibiotic (Fig. 3C). The K_D was calculated to be 5.4 ± 1.3 µM (Fig. 3D), which is larger than in the reverse configuration. Two explanations can account for this finding: i) the multivalency effect on the Van-modified surface may still be present despite precautions taken to limit the Van amount used in the

SELEX, and/or ii) surface steric hindrance if the binding pocket of the aptamer is near the 5' end, which is used for aptamer immobilization (discussed in section 3.3). Even though K_D shifted from the nM to the μM range, the applicability of this aptamer for TDM remains valid, given that the therapeutic range of Van is in the μM domain (the recommended trough concentration is 15–20 μg/mL Van, which is ~10–13.5 μM) [34].

Currently, there are only two SELEX studies reported in the literature, both employing Capture-SELEX for selecting aptamers targeting Van [26,35]. The aptamer developed by Dauphin-Ducharme et al., which is widely used in clinical scenarios, has an electrochemically determined K_D of 45.5 ± 2.2 μM [26]. This sequence was further optimized by truncation, improving the affinity up to 19.5 ± 1.6 μM, determined by isothermal titration calorimetry (ITC) [36]. A more recent study employed a modified Capture-SELEX approach incorporating fluorescence-activated cell sorting technique, obtaining 80 nt long sequences with K_D values via ITC ranging from 37.8 to 121 μM. Further truncation of these aptamers did not consistently improve their affinity, with the resulting K_D values between 50 and 174 μM [35]. Table S5 summarizes the main features of the Van-binding receptors, including aptamers and peptides, reported so far. Our aptamers, without any post-SELEX optimization, show higher affinity and could serve as potential alternatives for designing aptasensors for therapeutic monitoring of Van.

3.3. Computational modeling of 8H

According to mfold, 8H features two consecutive hairpin motifs formed by residues G6-C26 and G27-C39 (Figure S6). Both hairpins stay structurally stable during the cMD simulation, presenting moderate Root Mean Squared Deviation (RMSD) values and abundant (94–100 %) base pair canonical interactions in the stem regions (Figure S7 and Table S6). In contrast, the RMSD plot computed for the full aptamer displays a remarkable structural evolution during the cMD simulation due to the mutual reorientation of both hairpins. To show this rearrangement, Fig. 2B presents the cluster representatives of the two most populated clusters superposed considering the backbone heavy atoms in the first hairpin, and with a magenta line displaying the shift of A35 located in hairpin-2 (additional cluster representatives are collected in Figure S8). Thus, at the beginning of the simulation, the loop region in hairpin-2 is located close to the 5′-end due to G2•••T32 (26 % of abundance in the cMD trajectory) and G4•••A35 (25 %) stacking interactions observed in clusters #1 and #4. This initial arrangement evolves to give an alternative T3•••A35 stack (23 %), as characterized in clusters #2, #6, and #7 that populate the 2.5–5.0 μs interval. During the second half of the simulation, the G27-G45 moiety of 8H reorients with respect to the T1-C26 one and, for instance, a G5•••G42 base pair (22 %) and a G4•••T43 stacking contact (21 %) are present in the most abundant cluster #0 conformation. Concerning the terminal fragments, the 3′-end (C40-G35) is stably folded, forming a turn characterized by a highly abundant C40•••G45 Watson-Crick base pair (97 %), and its relative position is linked to that of hairpin-2 thanks to a G27•••G45 stacking interaction (96 % in Table S7). In contrast, the residues at the 5′-end (T1-G5) behave as a disordered coil, presenting only stacking interactions with each other with variable abundances in the range 40–97 % (see Table S7).

To gain insight into the binding mode between the 8H aptamer and Van, we conducted docking calculations (Van 3D structure in Figure S9). Interaction energies from the 300 more favorable poses of the 8H-Van complex ranged between −16.3 and −11.5 kcal/mol. Considering the six most favored 8H-Van complexes shown in Figure S10, it arises that Van binds 8H preferentially at the stem region of hairpin-1 (G6-A10, T22-C26), interacting also with some residues from the stem of hairpin-2 and/or from the 5′ or 3′-ends. However, the exact binding mode depends on the relative arrangement of the two hairpins, and on the conformation adopted by the highly flexible 5′-end. Interestingly, the structure of 8H in the most favored pose shown in Fig. 2B corresponds to that of cluster #0, sampled during the last four μs of the cMD simulation of the aptamer. But the small energy difference between this pose and the others in Figure S10 (<1.6 kcal/mol), does not allow us to be conclusive in selecting one docking model for the 8H-Van complex. Moreover, the flexibility characterized for the unbound 8H aptamer in solution suggests that some degree of induced fit, associated to the folding of hairpin-2 with respect to hairpin-1, may occur during the binding process. In this way, additional contacts to those shown in Fig. 2B would contribute to stabilize the complex.

3.4. Electrochemical aptasensing of Van

3.4.1. Aptasensor design and optimization

To validate the specific recognition and binding properties of the selected 8H aptamer, an electrochemical sensing platform was designed on disposable AuSPE. The thiolated 8H_1 aptamer was chemisorbed onto the surface, which was then blocked using *p*-ATP, as shown in Fig. 4A. Using a 2 μM 8H_1 concentration and blocking with 1 mM *p*-ATP, the fabrication process was monitored by DPV (Figure S11) with 5 mM $[Fe(CN)_6]^{4-/3-}$ in 0.1 M KCl as a soluble redox indicator. The current decreased after each modification and after interaction with 50 μM Van, demonstrating the recognition ability of the aptamer because of impeded electron transfer.

We compared two different methods for SAM preparation: passive incubation (IC) at RT and multipulse amperometry (MPA)-assisted deposition. Both methods yielded comparable signal decreases (30.2 ± 2.9 % for IC vs. 32.3 ± 0.8 % for MPA). However, given the significantly shorter immobilization time (1 h vs. 1 min), MPA was preferred. Aptamer coverage is critical for optimal performance. We tested three different concentrations (1, 2 and 5 μM). While the decrease in current was slightly higher at 2 μM than at 5 μM (Fig. 4B, blue bars), the interaction with 50 μM Van showed marked differences between the two coverages. The signal change at 5 μM of aptamer was 6.2-fold lower than at 2 μM, indicating that high coverage hinders the aptamer-Van binding (Fig. 4B, red columns). Based on these results, the 2 μM 8H_1 aptamer concentration was considered optimal and used for further sensor fabrication.

Non-specific adsorption is an undesirable but a common issue when analyzing clinical samples. We used an aromatic thiol instead of the standard alkanethiols for backfilling because it offers several advantages, particularly for small-molecule targets such as Van. They include enhanced electrical conductivity due to the aromatic ring and structural rigidity which enables a tailored organization of the SAM components [37]. The anti-biofouling properties of *p*-ATP may contribute to a lower background current compared to standard MCH [38]. Several *p*-ATP concentrations (1, 5 and 10 mM) and MPA blocking times (60, 120 and 180 s) were evaluated. Increasing both parameters reduced the accessibility of the redox probe to the electrode surface and decreased the current drastically (up to 83.7 ± 1.4 %, when 10 mM MPA was used for 60 s, Fig. 4C). Using 1 mM *p*-ATP as optimal concentration, we selected a time of 120 s as a balance to obtain measurable currents while effectively blocking the nonspecific adsorption. Indeed, the percentage of signal change for 10 μM Van was higher when *p*-ATP was immobilized for 60 s compared to 120 s (19.6 ± 3.2 % vs. 13.6 ± 1.0 %; Fig. 4D). However, the control aptasensor without aptamer (covered only with 1 mM *p*-ATP) exhibited better antifouling properties at 120 s (1.3 ± 0.7 % vs. 9.8 ± 1.5 % obtained at 60 s), so it was selected.

Finally, we found that the optimal incubation time of Van, tested at 50 μM, was 30 min after which the equilibrium was reached (Fig. 4E).

3.4.2. Analytical performance of the aptasensor

The proposed electrochemical aptasensor was challenged to increasing concentrations of Van under optimal experimental conditions. As shown in Fig. 4F, a concentration-dependent change in the signal was observed in the 2.5–50 μM concentration range. The analytical signal, expressed as $\Delta I/I_0$ (%), displayed a linear relationship with the logarithm of the Van concentration, with the following linear

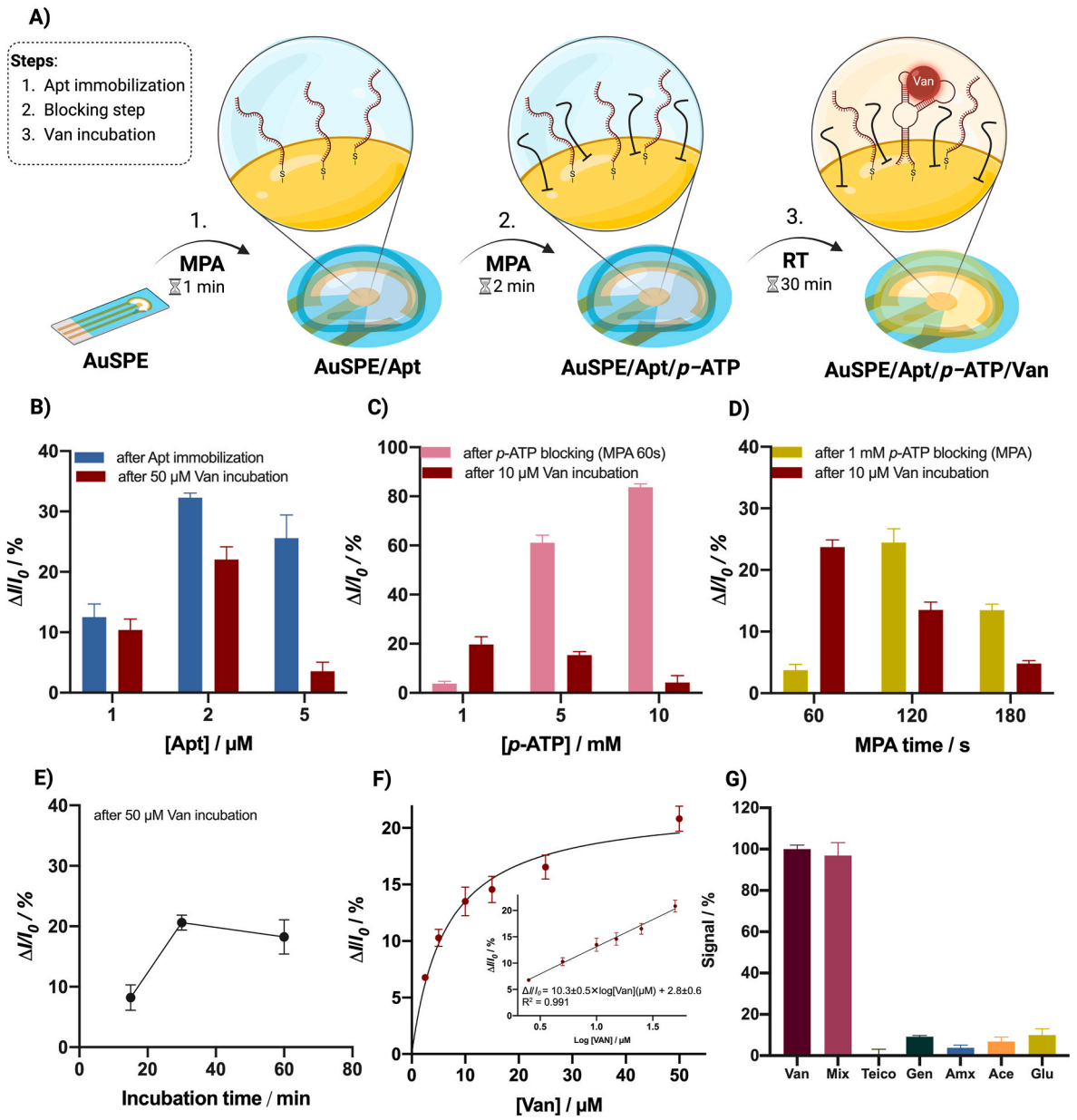

Fig. 4. A) Schematic representation of aptasensor fabrication process. Evaluation of the influence of **B)** 8H_1 concentration, **C)** *p*-ATP concentration, **D)** *p*-ATP deposition time through MPA and **E)** target interaction time on Van assessment. The bars represent the change in DPV current expressed as percentage (difference between the current after and the current before the step of interest divided by the current measured before). **F)** Percentage of DPV current change as a function of the Van concentration (2.5–50 µM). Inset: Linear relationship between the percentage of current change and the logarithm of Van concentration. **G)** Interference studies: the percentage of current change for 10 µM Van was considered 100 %. The percentage of current change in the presence of 10 µM interferent alone (Gentamicin - Gen, Amoxicillin – Amx, Acetaminophen – Ace, Glucose – Glu) or in the mixture with 10 µM Van (10 µM each) was then measured and expressed as percentage of the value measured with Van only. Glu was interrogated at physiological levels (500 µM) both alone and in the mixture. Error bars represent the standard deviation calculated from three different aptasensors.

regression equation: $\Delta I/I_0$ (%) = 10.3 ± 0.5 × log [Van] (µM) + 2.8 ± 0.6, R^2 = 0.991. The limit of detection was estimated to be 1.5 µM considering the logarithmic relationship and using equation (3) × σ/S, where σ represents the standard deviation of the regression equation and S is the slope.

Given the optimal Van trough serum concentrations (15–20 mg/L or 10.10–13.46 µM), the developed aptasensor is well-suited for TDM. Its calibration within a clinically relevant concentration range enables the quantification of both sub- and supratherapeutic Van levels. The fluorescent aptasensor recently developed with a novel aptamer showed similar analytical features (1–20 µM in buffer) The suitability to detect Van in the therapeutic level was demonstrating achieving a LOD in serum of 3.7 µM. This aptasensor relies on the strand displacement triggered by the Van recognition. It requires 10 min to complete and an extra DNA probe labeled with a quencher molecule [35].

The selectivity of the prepared aptasensor for Van was evaluated by measuring its response to potentially interfering drugs commonly administered to patients undergoing Van treatment, based on records from ten hospitalized patients. These included Gen, Amx and Ace. Additionally, Teico was tested to assess the ability of the aptamer to differentiate between structural analogs. Each interferent was tested at a concentration of 10 µM, following the same experimental conditions. To ensure the sensor suitability for serum analysis, physiological levels of Glu (500 µM) were also tested. The percentage of signal change at 10 µM

Van was considered as 100 %, and the responses to individual interferents were expressed relative to this value. All interfering molecules produced signal variations below 10 % (9.1 ± 0.6 % for Gen, 3.9 ± 1.3 % for Amx, 6.9 ± 2.3 % for Ace, −0.5 ± 3.7 % Teico, and 10 ± 3.1 % for Glu), confirming the high selectivity of the aptasensor towards Van (Fig. 4G).

Moreover, when the aptasensor was incubated with a mixture of Van with all the above-mentioned interferents, only a minor variation was observed compared to the signal obtained for 10 μM Van alone (96.9 ± 6.3 %), suggesting no significant interferences (Student's *t*-test; $p = 0.915 > 0.05$). While the simultaneous presence of all these interferents in the serum is uncommon, this approach was employed to rigorously assess the specificity of the aptamer.

For stability assessment, aptasensors were fabricated and stored at 4 °C in water-saturated atmosphere, with their surface covered by 50 μL of PBS buffer, to prevent dehydration. The sensors were then tested for their ability to detect 10 μM Van after 1, 3, 5 and 7 days of storage (Figure S12A). The electrochemical response in DPV ($\Delta I/I_0$ (%)), remained consistent after 24 h of storage (~4 % observed decrease), indicating good short-term storage stability under refrigerated conditions. After 3 days, the signal decreased considerably (~20 %), suggesting degradation of the aptasensor. This trend was further observed after 5 and 7 days of incubation, with the DPV signal decreasing to a maximum of ~30 %, suggesting further degradation while still maintaining suitability for measurement. Regarding batch-to-batch reproducibility, the response of five independently prepared aptasensor was evaluated (Figure S12B). The current response toward 10 μM Van was compared across the batches and the results showed acceptable reproducibility with minimal variation in signal output (RSD = 3.5 %), supporting the robustness of the fabrication protocol.

3.4.3. *Applicability in human serum*

To evaluate the performance of the aptasensor in more complex biological matrices, commercial serum was spiked with various concentrations of Van (10, 15 and 25 μM) and subsequently analyzed. The aptasensor was first incubated in unspiked serum to establish the blank current, followed by incubation in spiked serum. The change in the blank current signal was subtracted from the signal obtained for the spiked samples, and the resulting difference was used to determine the Van concentration based on the regression equation of the calibration plot. The recovery rates ranged from 89 % to 110 % with a maximum RSD of 5.2 % (Table S8). These results demonstrate that 8H aptamer effectively recognizes and binds Van even in complex media.

Next, serum samples from 10 patients undergoing Van treatment were analyzed. Table 1 shows that the concentrations of Van in the serum samples obtained with the aptasensor are in good agreement with the results of the standard method used in clinics (PETINIA) (Figure S12, $R^2 = 0.994$). A two-tailed paired *t*-test was conducted to compare the Van concentrations obtained using PETINIA and the electrochemical aptasensor across the serum samples. There was no statistically significant difference between the two methods ($p = 0.6943 > 0.05$).

Table 1
Comparison of Van levels obtained in human serum samples by standard method (PETINIA) and the developed electrochemical aptasensor.

Patient	PETINIA (μM)	Aptasensor (μM)	Relative trueness[a] (%)
1	12.9	11.7 ± 1.5	90.4
2	7.1	6.5 ± 0.6	91.1
3	9.7	10.1 ± 0.6	104.2
4	7.5	7.6 ± 0.7	100.4
5	13.4	14.7 ± 0.1	109.6
6	20.7	17.7 ± 2.5	85.5
7	15.8	16.7 ± 0.6	106.1
8	17.4	18.0 ± 2.4	103.3
9	26.3	25.7 ± 1.6	97.9
10	16.0	16.5 ± 2.1	103.5

[a] Calculated as 100-relative error.

These results serve as a proof-of-concept to validate the capability of the developed aptasensor to detect Van directly in real clinical samples rather than in artificial matrices or spiked controls. Despite the limited sample size, the aptasensor was able to stratify Van concentrations in the clinically relevant range, supporting its potential for guiding therapeutic decisions. However, broader clinical validation is essential to fully assess the robustness and generalizability of the platform. Future studies will expand to larger patient cohorts and consider potential interfering factors, such as inter-patient variability, clinical history, medication, and hydration status, which may influence the sensor's response and Van concentration. Additionally, further optimization of the electrochemical sensing platform by incorporating nanomaterials [39] with high electrical conductivity and signal amplification strategies [40,41] to enhance sensitivity might reduce the required incubation time and improve the current LOD, thus improving its suitability for point-of-care applications by faster analysis time and reliability under various physiological conditions, particularly in sub-therapeutic scenarios. Finally, this work lays a conceptual foundation for translating the aptasensor technology into clinical settings. This must be supported by further miniaturization using portable potentiostats, assessment of the ability to detect Van in whole blood and validation through larger-scale clinical trials.

While HPLC-MS is the primary technique employed for Van TDM due to its high sensitivity and selectivity, it presents several limitations, including the requirement for expensive instrumentation, the need for trained personnel to perform complex operations, laborious sample pretreatment which can extend the analysis time. Immunoassays are increasingly used in clinical settings owing to their high sensitivity and specificity, which are based on competitive antibody binding. The availability of commercial reagent kits and a high degree of automation with simple and rapid workflows are clear advantages for TDM. However, immunoassays are susceptible to interference from matrix components, co-administered drugs and metabolites. Additionally, the limited thermal and chemical stability of antibodies, along with their high production costs, remain significant drawbacks [42,43]. Recently, some concerns about finding falsely low Van concentrations using PETINIA method have been raised and associated with alterations of turbidity caused by free kappa light chains [44]. The electrochemical aptasensor can skip this drawback, offering a fast, sensitive, user-friendly and cost-effective alternative for Van TDM.

4. Conclusions

In this study, we show that when the small target molecule has at least one suitable functional group for binding, MBs-SELEX is a simpler and faster approach than capture SELEX for obtaining reliable aptamers with affinity in the submicromolar range, requiring approximately half the number of selection rounds. We observed a significant difference in the apparent binding constant depending on the configuration of the assay, that is, the molecule attached. This suggests an "avidity effect" that occurs when the target is immobilized, despite efforts to limit the amount of Van in the selection. It is apparent that further reducing the amount of Van could help completely eliminate this effect. The affinity in the configuration used for the aptasensor is slightly better than the first Van aptamer and one-order of magnitude better than the recently raised Van aptamer after truncation, supporting calibration within the clinically relevant range. The APTAMD computational protocol and docking calculations provide us with a reliably obtained 3D structure for the selected aptamer and several models for its complex with Van that systematically point to the binding in the region connecting hairpins 1 and 2. The direct, unlabeled assay proposed for Van quantification does not rely on strong conformational changes. This means that aptamer truncation is not strictly necessary for functionality and measurable signal generation. The aptasensor performance was successfully validated in clinical samples from hospitalized patients undergoing Van

treatment, showing strong agreement with the clinical standard immunoassay. This study serves as a foundation for on-site TDM using electrochemical sensors, providing a rapid and accurate tool for personalized medicine and real-time dose adjustments without the need of waiting for centralized overcrowded analysis. We envision improved performance using nanostructured electrode surfaces.

CRediT authorship contribution statement

Magdolna Casian: Writing – review & editing, Writing – original draft, Validation, Methodology, Investigation, Formal analysis, Conceptualization. **Oana Hosu-Stancioiu:** Writing – review & editing, Writing – original draft, Methodology, Funding acquisition, Formal analysis, Conceptualization. **Ioana Manea:** Writing – review & editing, Writing – original draft, Investigation, Formal analysis, Data curation. **Dimas Suárez:** Writing – original draft, Visualization, Software, Investigation. **Natalia Díaz:** Writing – review & editing, Visualization, Software, Investigation. **María Jesús Lobo Castañón:** Writing – review & editing, Visualization, Supervision, Funding acquisition. **Noemí de-los-Santos-Álvarez:** Writing – review & editing, Supervision, Resources, Project administration, Conceptualization. **Cecilia Cristea:** Writing – review & editing, Supervision, Resources, Funding acquisition, Conceptualization.

Informed consent statement

Informed consent was obtained from all subjects involved in the study.

Ethics declarations

The study was conducted in accordance with the Declaration of Helsinki and was approved by the Ethics Committee of the Cluj-Napoca Municipal Clinical Hospital (No. 1/16.02.2024), and "Iuliu Haţieganu" University of Medicine and Pharmacy Cluj-Napoca (No. 119/04.06.2024).

Declaration of competing interest

The authors declare that they have no known competing financial interests or personal relationships that could have appeared to influence the work reported in this paper.

Acknowledgments/Funding

This work was supported by European Union's Horizon Europe research and innovation program under the grant agreement "European integration of new technologies and social-economic solutions for increasing consumer trust and engagement in seafood products" (FishEuTrust), Grant Agreement: 101060712/20-22, grant of Romanian Ministry of Education and Research PN-IV-P8-8.1-PRE-HE-ORG-2023-0076 contract no. 26 PHE/2022, Spanish Government Project PID2021-123183OB-100 MICIN/AEI/10.13039/501100011033/FEDER UE, RED2022-134120-T and Principado de Asturias Government (IDE/2024/000677). MC acknowledges Iuliu Haţieganu UMF for internal grant no. 779/1/13.01.2025. The authors kindly acknowledge clinical pharmacist Ligia Hui from Cluj-Napoca Municipal Clinical Hospital for her assistance regarding subject inclusion and serum sample collection.

Appendix A. Supplementary data

Supplementary data to this article can be found online at https://doi.org/10.1016/j.aca.2025.344519.

Data availability

Data will be made available on request.

References

[1] C.J. Graham, The global threat of antibiotic resistance: what can be done? J. Glob. Health Rep. 1 (2017) e2017002 https://doi.org/10.29392/joghr.1.e2017002.
[2] M. Zhuang, Y. Achmon, Y. Cao, X. Liang, L. Chen, H. Wang, B.A. Siame, K.Y. Leung, Distribution of antibiotic resistance genes in the environment, Environ. Pollut. 285 (2021) 117402, https://doi.org/10.1016/j.envpol.2021.117402.
[3] A. Cafaro, S. Barco, F. Pigliasco, C. Russo, M. Mariani, A. Mesini, C. Saffioti, E. Castagnola, G. Cangemi, Therapeutic drug monitoring of glycopeptide antimicrobials: an overview of liquid chromatography-tandem mass spectrometry methods, J. Mass Spectrom. Adv. Clin. Lab 31 (2024) 33–39, https://doi.org/10.1016/j.jmsacl.2023.12.003.
[4] A. Cafaro, M. Conti, F. Pigliasco, S. Barco, R. Bandettini, G. Cangemi, Biological fluid microsampling for therapeutic drug monitoring: a narrative review, Biomedicines 11 (2023) 1962, https://doi.org/10.3390/biomedicines11071962.
[5] A. Dasgupta, Advances in antibiotic measurement, Adv. Clin. Chem. 56 (2012) 75–104, https://doi.org/10.1016/b978-0-12-394317-0.00013-3.
[6] E. Rubinstein, Y. Keynan, Vancomycin revisited - 60 years later, Front. Public Health 2 (2014) 77697, https://doi.org/10.3389/fpubh.2014.00217.
[7] C.Y. Chen, M.Y. Li, L.Y. Ma, X.Y. Zhai, D.H. Luo, Y. Zhou, Z.M. Liu, Y.M. Cui, Precision and accuracy of commercial assays for vancomycin therapeutic drug monitoring: evaluation based on external quality assessment scheme, J. Antimicrob. Chemother. 75 (2020) 2110–2119, https://doi.org/10.1093/jac/dkaa150.
[8] R. Zonozi, A. Wu, J.I. Shin, A. Secora, J. Coresh, L.A. Inker, A.R. Chang, M. E. Grams, Elevated vancomycin trough levels in a tertiary health system: frequency, risk factors, and prognosis, Mayo Clin. Proc. 94 (2019) 17, https://doi.org/10.1016/j.mayocp.2018.08.034.
[9] X. Liang, Y. Fan, M. Yang, J. Zhang, J. Wu, J. Yu, J. Tao, G. Lu, H. Zhang, R. Wang, X. Wen, H. Li, F. Zhang, J. Hang, L. Shen, Z. Zhang, Q. Lin, F. Fu, S. Wu, B. Shen, W. Huang, C. Chang, H. Zhang, Q. Huang, Y. Shi, H. Ren, Q. Yuan, X. Song, X. Luo, A prospective multicenter clinical observational study on vancomycin efficiency and safety with therapeutic drug monitoring, Clin. Infect. Dis. 67 (2018) S249–S255, https://doi.org/10.1093/cid/ciy680.
[10] J.L. Crandon, S.H. MacVane, D.P. Nicolau, Clinical laboratory–based assay methodologies may underestimate and increase variability of vancomycin protein binding in hospitalized patients, Pharmacotherapy 34 (2014) 203–209, https://doi.org/10.1002/PHAR.1323.
[11] L. Scribel, A. Galiotto, I. de S. Rodrigues, R. Hahn, R. Linden, A.P. Zavascki, Comparison of vancomycin assays in patients undergoing hemodialysis, Braz. J. Infect. Dis. 28 (2024) 103869, https://doi.org/10.1016/j.bjid.2024.103869.
[12] F.R. Vidal, D.S. Ossanes, L. Birk, C. Scheid, F.S. Barbosa, E. Dallegrave, J. Merib, S. Eller, T.F. de Oliveira, Development and validation of a dried plasma spot LC–MS/MS method for therapeutic monitoring of vancomycin and comparison with enzyme-multiplied immunoassay, Biomed. Chromatogr. 37 (2023) e5586, https://doi.org/10.1002/bmc.5586.
[13] D.F. Legatt, G.B. Blakney, T.N. Higgins, K.L. Schnabl, C.E. Shalapay, V.C. Dias, J. C. Wesenberg, The effect of paraproteins and rheumatoid factor on four commercial immunoassays for vancomycin: implications for laboratorians and other health care professionals, Ther. Drug Monit. 34 (2012) 306–311, https://doi.org/10.1097/FTD.0b013e318257335f.
[14] M. Arabyat, A. Abdul-Sattar, F. Al-Fararjah, A. Al-Ghazawi, A. Rabayah, R. Al-Hasassnah, W. Mohmmad, I. Al-Adham, S. Hamadi, N. Idkaidek, Therapeutic drug monitoring of vancomycin in Jordanian patients. Development of physiologically-based pharmacokinetic (PBPK) model and validation of class II drugs of salivary excretion classification system (SECS), Drug Res. 72 (2022) 441–448, https://doi.org/10.1055/A-1852-5391.
[15] X. Jiang, Y. Qin, R. Lei, Y. Han, J. Yang, G. Zhang, J. Liu, A rapid and simple HPLC-MS/MS method for the therapeutic drug monitoring of six special-grade antimicrobials in pediatric patients, Heliyon 10 (2024) e24198, https://doi.org/10.1016/j.heliyon.2024.e24198.
[16] G. Yuan, H. Liu, A.S. Shaikh, R. Zhang, P. Li, B. Wang, R. Guo, Comparison of new liquid chromatography-mass spectrometry method and enzyme-multiplied immunoassay technique for routine therapeutic drug monitoring of vancomycin in Chinese patients, Clin. Lab. 64 (2018) 277–285, https://doi.org/10.7754/Clin.Lab.2017.170926.
[17] A.D. Ellington, J.W. Szostak, In vitro selection of RNA molecules that bind specific ligands, Nature 346 (1990) 818–822, https://doi.org/10.1038/346818a0, 1990.
[18] C. Tuerk, L. Gold, Systematic evolution of ligands by exponential enrichment: RNA ligands to bacteriophage T4 DNA polymerase, Science 249 (1990) 505–510, https://doi.org/10.1126/science.2200121.
[19] G. Ştefan, O. Hosu, K. De Wael, M.J. Lobo-Castañón, C. Cristea, Aptamers in biomedicine: selection strategies and recent advances, Electrochim. Acta 376 (2021) 137994, https://doi.org/10.1016/j.electacta.2021.137994.
[20] R.K. Mosing, M.T. Bowser, Isolating aptamers using capillary Electrophoresis–SELEX (CE–SELEX), in: G. Mayer (Ed.), Nucleic Acid and Peptide Aptamers, Methods in Molecular Biology, Humana Press, Totowa, NJ, 2009, pp. 33–43, https://doi.org/10.1007/978-1-59745-557-2_3.

[21] K. Sefah, D. Shangguan, X. Xiong, M.B. O'Donoghue, W. Tan, Development of DNA aptamers using Cell-SELEX, Nat. Protoc. 5 (2010) 1169–1185, https://doi.org/10.1038/nprot.2010.66.
[22] A. Sinha, P. Gopinathan, Y. Da Chung, H.Y. Lin, K.H. Li, H.P. Ma, P.C. Huang, S. C. Shiesh, G. Bin Lee, An integrated microfluidic platform to perform uninterrupted SELEX cycles to screen affinity reagents specific to cardiovascular biomarkers, Biosens. Bioelectron. 122 (2018) 104–112, https://doi.org/10.1016/j.bios.2018.09.040.
[23] Y. Ding, J. Liu, Quantitative comparison of Capture-SELEX, GO-SELEX, and Gold-SELEX for enrichment of aptamers, Anal. Chem. 95 (2023) 14651–14658, https://doi.org/10.1021/acs.analchem.3c02477.
[24] R. Stoltenburg, C. Reinemann, B. Strehlitz, FluMag-SELEX as an advantageous method for DNA aptamer selection, Anal. Bioanal. Chem. 383 (2005) 83–91, https://doi.org/10.1007/s00216-005-3388-9.
[25] I. Manea, M. Casian, O. Hosu-Stancioiu, N. de-los-Santos-Álvarez, M.J. Lobo-Castañón, C. Cristea, A review on magnetic beads-based SELEX technologies: applications from small to large target molecules, Anal. Chim. Acta 1297 (2024) 342325, https://doi.org/10.1016/j.aca.2024.342325.
[26] P. Dauphin-Ducharme, K. Yang, N. Arroyo-Currás, K.L. Ploense, Y. Zhang, J. Gerson, M. Kurnik, T.E. Kippin, M.N. Stojanovic, K.W. Plaxco, Electrochemical aptamer-based sensors for improved therapeutic drug monitoring and high-precision, feedback-controlled drug delivery, ACS Sens. 4 (2019) 2832, https://doi.org/10.1021/acssensors.9b01616.
[27] Y. Liu, J.O. Mack, M. Shojaee, A. Shaver, A. George, W. Clarke, N. Patel, N. Arroyo-Currás, Analytical validation of aptamer-based serum vancomycin monitoring relative to automated immunoassays, ACS Sens. 9 (2024) 228–235, https://doi.org/10.1021/acssensors.3c01868.
[28] A. Díaz-Fernández, C.S. Ciudad, N. Díaz, D. Suárez, N. de-los-Santos-Álvarez, M. J. Lobo-Castañón, Refinement and truncation of DNA aptamers based on molecular dynamics simulations: computational protocol and experimental validation, ChemRxiv (2025), https://doi.org/10.26434/chemrxiv-2025-k5mzk. This content is a preprint and has not been peer-reviewed.
[29] D.A. Case, H.M. Aktulga, K. Belfon, I.Y. Ben-Shalom, J.T. Berryman, S.R. Brozell, D. S. Cerutti, T.E. Cheatham III, G.A. Cisneros, V.W.D. Cruzeiro, T.A. Darden, R. E. Duke, G. Giambasu, M.K. Gilson, H. Gohlke, A.W. Goetz, R. Harris, S. Izadi, S. A. Izmailov, K. Kasavajhala, M.C. Kaymak, E. King, A. Kovalenko, T. Kurtzman, T. S. Lee, S. LeGrand, P. Li, C. Lin, J. Liu, T. Luchko, R. Luo, M. Machado, V. Man, M. Manathunga, K.M. Merz, Y. Miao, O. Mikhailovskii, G. Monard, H. Nguyen, K. A. O'Hearn, A. Onufriev, F. Pan, S. Pantano, R. Qi, A. Rahnamoun, D.R. Roe, A. Roitberg, C. Sagui, S. Schott-Verdugo, A. Shajan, J. Shen, C.L. Simmerling, N. R. Skrynnikov, J. Smith, J. Swails, R.C. Walker, J. Wang, J. Wang, H. Wei, R. M. Wolf, X. Wu, Y. Xiong, Y. Xue, D.M. York, S. Zhao, P.A. Kollman, Amber 2022, University of California, San Francisco, 2022.
[30] G.M. Morris, R. Huey, W. Lindstrom, M.F. Sanner, R.K. Belew, D.S. Goodsell, A. J. Olson, AutoDock4 and AutoDockTools4: automated docking with selective receptor flexibility, J. Comput. Chem. 30 (2009) 2785–2791, https://doi.org/10.1002/jcc.21256.
[31] M. Zuker, Mfold web server for nucleic acid folding and hybridization prediction, Nucleic Acids Res. 31 (2003) 3406–3415, https://doi.org/10.1093/nar/gkg595.
[32] K. Darty, A. Denise, Y. Ponty, VARNA: interactive drawing and editing of the RNA secondary structure, Bioinformatics 25 (2009) 1974–1975, https://doi.org/10.1093/bioinformatics/btp250.
[33] R. Lorenzo-Gómez, R. Miranda-Castro, J.R. de los Toyos, N. de-los-Santos-Álvarez, M.J. Lobo-Castañón, Aptamers targeting a tumor-associated extracellular matrix component: the human mature collagen XIα1, Anal. Chim. Acta 1189 (2022) 339206, https://doi.org/10.1016/j.aca.2021.339206.
[34] M. Rybak, B. Lomaestro, J.C. Rotschafer, R. Moellering, W. Craig, M. Billeter, J. R. Dalovisio, D.P. Levine, Therapeutic monitoring of vancomycin in adult patients: a consensus review of the American Society of Health-System Pharmacists, the Infectious Diseases Society of America, and the Society of Infectious Diseases Pharmacists, Am. J. Health Syst. Pharm. 66 (2009) 82–98, https://doi.org/10.2146/ajhp080434.
[35] X. Fang, T. Gao, Z. Luo, R. Pei, Efficient selection of vancomycin-specific aptamers via particle display and development of a high-sensitivity fluorescent apta-sensor for vancomycin detection, Sensor. Actuator. B Chem. 436 (2025) 137681, https://doi.org/10.1016/j.snb.2025.137681.
[36] A. Shaver, J.D. Mahlum, K. Scida, M.L. Johnston, M. Aller Pellitero, Y. Wu, G. V. Carr, N. Arroyo-Currás, Optimization of Vancomycin aptamer sequence length increases the sensitivity of electrochemical, aptamer-based sensors in vivo, ACS Sens. 7 (2022) 3895–3905, https://doi.org/10.1021/acssensors.2c01910.
[37] R. Miranda-Castro, R. Sánchez-Salcedo, B. Suárez-Álvarez, N. De-los-Santos-Álvarez, A.J. Miranda-Ordieres, M.J. Lobo-Castañón, Thioaromatic DNA monolayers for target-amplification-free electrochemical sensing of environmental pathogenic bacteria, Biosens. Bioelectron. 92 (2017) 162–170, https://doi.org/10.1016/j.bios.2017.02.017.
[38] S. Campuzano, M. Pedrero, P. Yáñez-Sedeño, J.M. Pingarrón, Antifouling (Bio) materials for electrochemical (Bio)sensing, Int. J. Mol. Sci. 20 (2019) 423, https://doi.org/10.3390/ijms20020423.
[39] N.S. Alsaiari, K.M.M. Katubi, F.M. Alzahrani, S.M. Siddeeg, M.A. Tahoon, The application of nanomaterials for the electrochemical detection of antibiotics: a review, Micromachines 12 (2021) 308, https://doi.org/10.3390/mi12030308.
[40] A. Rhouati, J.L. Marty, A. Vasilescu, Electrochemical biosensors combining aptamers and enzymatic activity: challenges and analytical opportunities, Electrochim. Acta 390 (2021) 138863, https://doi.org/10.1016/j.electacta.2021.138863.
[41] Y. Liu, J. Canoura, O. Alkhamis, Y. Xiao, Immobilization strategies for enhancing sensitivity of electrochemical aptamer-based sensors, ACS Appl. Mater. Interfaces 13 (2021) 9491–9499, https://doi.org/10.1021/acsami.0c20707.
[42] Z. Fang, H. Zhang, J. Guo, J. Guo, Overview of therapeutic drug monitoring and clinical practice, Talanta 266 (2024) 124996, https://doi.org/10.1016/j.talanta.2023.124996.
[43] A. Pollap, J. Kochana, Electrochemical immunosensors for antibiotic detection, Biosensors 9 (2019) 61, https://doi.org/10.3390/bios9020061.
[44] N.Y. Tang, K. Walewski, R. Carey-Ballough, E. Sykes, Q. Sun, A suspected case of falsely low digoxin and vancomycin concentrations caused by free kappa light chains with PETINIA method, Pract. Lab. Med. 30 (2022) e00277, https://doi.org/10.1016/j.plabm.2022.e00277.